

Anatomy of unfolding: The site-specific fold stability of Yfh1 measured by 2D NMR

Rita Puglisi

UK-DRI at the Wohl Institute of King's College London, 5 Cutcombe Rd, SE59RT London (UK)

<https://orcid.org/0000-0002-2980-442X>

Gogulan Karunanithy

University College London

Flemming Hansen

University College London

Annalisa Pastore

King's College London <https://orcid.org/0000-0002-3047-654X>

Piero Temussi (✉ temussi@unina.it)

Dipartimento di Scienze Chimiche, Università di Napoli Federico II, Napoli, Italy <https://orcid.org/0000-0001-6032-4291>

Article

Keywords: biophysics, cold denaturation, NMR, protein stability, thermal unfolding, thermodynamics

Posted Date: May 6th, 2021

DOI: <https://doi.org/10.21203/rs.3.rs-484005/v1>

License:   This work is licensed under a Creative Commons Attribution 4.0 International License.

[Read Full License](#)

Version of Record: A version of this preprint was published at Communications Chemistry on September 6th, 2021. See the published version at <https://doi.org/10.1038/s42004-021-00566-3>.

1
2
3
4
5
6
7
8
9
10
11
12
13
14
15
16
17
18

Anatomy of unfolding: The site-specific fold stability of Yfh1 measured by 2D NMR

Rita Puglisi¹, Gogulan Karunanithy², D. Flemming Hansen², Annalisa Pastore^{1*}, Piero
Andrea Temussi^{1*}

¹UK-DRI at King’s College London, The Wohl Institute, 5 Cutcombe Rd, SE59RT London
(UK)

²Department of Structural Biology, Division of Biosciences, University College London,
London, UK, WC1E 6BT

*To whom correspondence should be addressed

annalisa.pastore@crick.ac.uk

temussi@unina.it

Keywords: biophysics, cold denaturation, NMR, protein stability, thermal unfolding,
thermodynamics

Running title: Site specific fold stability of Yfh1 by 2D NMR

19 **Abstract**

20 Most techniques allow detection of protein unfolding either by following the behaviour of
21 single reporters or as an averaged all-or-none process. We recently added 2D NMR
22 spectroscopy to the well-established techniques able to obtain information on the process of
23 unfolding using resonances of residues in the hydrophobic core of a protein. Here, we
24 questioned whether an analysis of the individual stability curves from each resonance could
25 provide additional site-specific information. We used the Yfh1 protein that has the unique
26 feature to undergo both cold and heat denaturation at temperatures above water freezing at low
27 ionic strength. We show that stability curves inconsistent with the average NMR curve from
28 hydrophobic core residues mainly comprise exposed outliers that do nevertheless provide
29 precious information. By monitoring both cold and heat denaturation of individual residues we
30 gain knowledge on the process of cold denaturation and convincingly demonstrate that the two
31 unfolding processes are intrinsically different.

32

33

34 **Introduction**

35 We are all accustomed to the concept that proteins unfold when temperature is increased. Less
36 well known is that all proteins unfold in principle also at low temperatures as demonstrated by
37 P. Privalov on purely thermodynamics grounds.¹ According to this theory, the driving force of
38 heat denaturation is the increase of conformational entropy with temperature. This
39 automatically involves the hydrophobic core and disfavours less ordered parts of the
40 architecture. On the contrary, while the mechanism of cold denaturation is still debated, the
41 current hypothesis is that this transition occurs when entropy decreases. In this case, the driving
42 force of unfolding would be driven by the sudden solvation of the hydrophobic residues of the
43 core.¹

44 The reason why cold denaturation is much less understood than the heat transition is that
45 most proteins undergo cold denaturation at temperatures below the water freezing point. This
46 is unfortunate because observation of both unfolding temperatures is in principle very valuable
47 as it allows calculation of reliable stability curves of the protein and of the whole set of
48 thermodynamic parameters.

49 We have identified a protein, Yfh1, that, as a full-length natural protein, undergoes cold
50 and heat denaturation at detectable temperatures when in the absence of salt.² We have
51 extensively exploited these properties to gain new insights both on the denatured states of
52 Yfh1³ and on the factors that may influence its stability.⁴ The value of Yfh1 as a tool to
53 investigate the unfolding process is evidenced not only by our subsequent work⁵⁻⁸ but also by
54 papers from other laboratories.⁹⁻¹²

55 In our studies, we noticed that most techniques employed to monitor protein stability are
56 however not “regiospecific”, as they yield a global result, *i.e.* an estimate of the stability of the
57 whole protein architecture, observable through the global evolution of secondary structure
58 elements upon an environmental insult. This is because we postulate an all-or-none cooperative
59 process in which the protein collapses altogether from a folded to an unfolded state. When
60 monitoring unfolding of a protein by CD spectroscopy, for instance, we observe intensity
61 changes related to the disruption of alpha helices and/or beta sheets under the influence of
62 physical or chemical agents.

63 It would instead be interesting to gauge the response of selected regions of the protein at
64 the single residue level to gain new insights into the mechanisms of unfolding of selected parts
65 of the protein structure. A technique ideally suited for this purpose is 2D ¹⁵N HSQC
66 spectroscopy since it provides a direct fingerprint of the protein through mapping each of the
67 amide protons. Volume variations of the NMR resonances may reflect changes affecting single

68 atoms of each residue and indirectly report on how they are individually affected by the
69 unfolding process. We recently showed, using Yfh1 as a suitable model, that it is possible to
70 use 2D NMR to measure protein stability and get thermodynamic parameters comparable to
71 those obtained by CD.¹³ We showed that this is possible provided that the residues chosen are
72 those buried in the hydrophobic core, thus experiencing the unfolding process directly. To
73 reliably select these residues, we introduced a parameter RAD which was defined as the
74 combination of the depth of an amide group from the protein surface and the relative
75 accessibility at the atom level.¹³ We demonstrated that, by excluding most of the exposed
76 residues (RAD values for the amide nitrogens ≥ 0.5) and averaging over resonances from
77 residues with RAD values lower than 0.1, we can obtain thermodynamics parameters
78 indistinguishable, within experimental error, from those obtained by CD or 1D NMR.¹³

79 Using the approach previously developed,¹³ we systematically analysed in the current
80 work the heat and cold denaturation of Yfh1 at residue detail but we reversed the perspective
81 and wondered what information, if any, would be carried by residues far from the hydrophobic
82 core and how they reflect the process of unfolding. This subject has increasingly attracted
83 attention: as put in the words of a recent study by Grassein et al.¹⁴: “For most of the proteins,
84 this global heat-induced denaturation curve can be formally described by a simple two-state
85 (folded/unfolded) statistical model. Agreement with a two-state model does not imply,
86 however, that the macromolecule does not unfold through a number of intermediate states....
87 Hence, the global denaturation curve hides the heterogeneity of protein unfolding. ...Local
88 nativeness is not uniquely defined and is probe dependent.” Understanding how individual
89 residues report on protein unfolding is also relevant in view of an increasing number of studies
90 on protein stability based on the intensity variations of the resonance of a single residue upon
91 unfolding.¹⁵⁻¹⁷ The excellent agreement between NMR and CD thermodynamic parameters
92 using 2D NMR¹³ put us in the position to examine the output of single residues critically and
93 follow the process of unfolding at an atomic level.

94 Using once again Yfh1, we show here that it is possible to sort out which individual
95 single residues yield stability curves consistent with the global unfolding process and that we
96 can obtain valuable information on the process of unfolding from residues that diverge from
97 the average behaviour: whereas some of the residues signal a single folding/unfolding event,
98 we find that others report on more complex thermodynamic events. Our data directly
99 demonstrate that the cold and heat denaturation processes have distinctly different mechanisms
100 and provide site-specific information on solvent interactions supporting Privalov’s
101 interpretation of cold denaturation.¹ Our results also clearly demonstrate the considerable

102 advantages of NMR over other approaches, such as in CD or fluorescence, that probe only bulk
103 transitions or individual residues.

104

105 **Results**

106 **Data collection and preliminary considerations**

107 To study the unfolding of Yfh1, we collected ^{15}N HSQC spectra of Yfh1 at different
108 temperatures and extracted the volumes of individual residues as a function of temperature
109 (**Figure S1 of Suppl. Mat.**). This could be confidently done for 68 (out of the expected 109)
110 well resolved resonances. The behaviour of ^{15}N HSQC spectra of Yfh1 as a function of
111 temperature was not uniform: some peaks could be observed nearly at all temperatures in the
112 range 273-323 K, others disappeared at temperatures intermediate between room temperature
113 and the two unfolding temperatures, *i.e.* lower than 323 K or higher than 273 K (**Figures S2**
114 **and S3 of Suppl. Mat.**). This behaviour can of course be ascribed to the exchange regime
115 (intermediate) between folded and unfolded conformations of these residues and told us that
116 they are not an integral part of the architecture of the folded form. The possibility that the
117 intensity changes in the HSQCs at low temperature could be solely due to exchange broadening
118 and not to unfolding can however be excluded by the practically perfect agreement between
119 the curves obtained by CD and by NMR (both 1D⁶ and 2D¹³). Cold denaturation of Yfh1 has
120 also been independently confirmed by five independent techniques.¹⁴⁻¹⁶

121

122 **Extraction of the thermodynamics parameters**

123 We could then extract the thermodynamic parameters of the unfolding process for the selected
124 resonance assuming that some conditions are met.^{1,4} We first assumed that unfolding transitions
125 are, at a first approximation, two-state processes from folded (F) to unfolded (U) states. We
126 then postulated that the difference of the heat capacity of the two forms (ΔC_p) does not depend
127 on temperature. This assumption is considered reasonable when the heat capacities of the native
128 and denatured states change in parallel with temperature variations.¹ When these two
129 conditions are reasonably met, the populations of the two states at temperature T, $f_F(T)$ and
130 $f_U(T)$, are a function of the Gibbs free energy of unfolding, $\Delta G^0(T)$ (see Methods and Martin
131 et al.).⁴ The plot of the free energy of unfolding as a function of temperature provides what is
132 called the stability curve of a protein.¹⁸ From this equation the main thermodynamic
133 parameters, *i.e.* heat melting temperature (T_m), enthalpy difference at the melting point (ΔH_m)
134 and the heat capacity difference at constant pressure (ΔC_p), can be determined using a non-

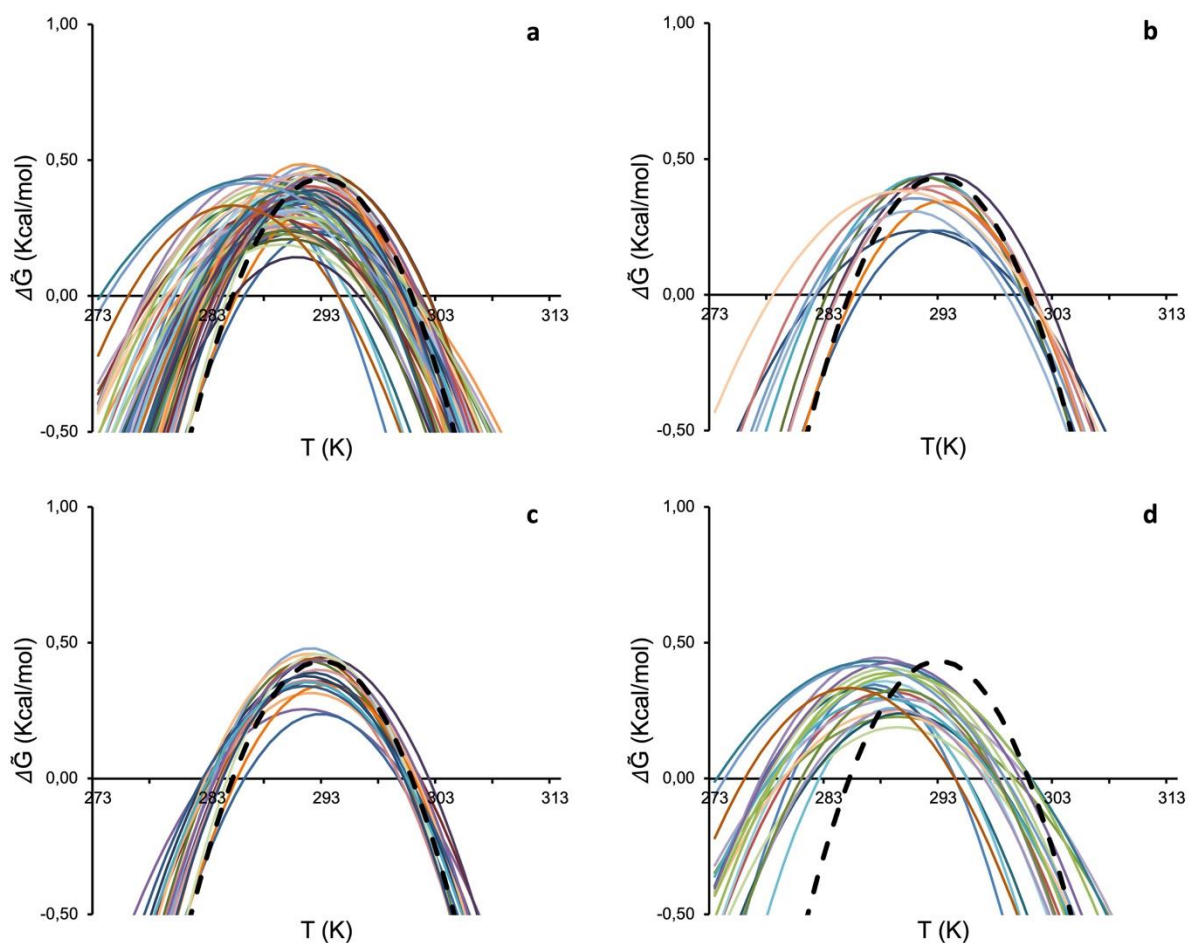
135 linear fit (damped least-squares method, also known as the Levenberg-Marquardt
136 algorithm).^{19,20} Other parameters, *e.g.* the low temperature unfolding (T_c), can be read from the
137 stability curve. When the original assumptions are significantly wrong, fitting results in
138 unrealistic numbers. In our case, the volumes were transformed into relative populations of
139 folded Yfh1 assuming that, as measured by CD and confirmed in other studies on Yfh1,^{2,4,7,8}
140 unfolded forms are in equilibrium with, on average, a 70% population of folded Yfh1 at room
141 temperature. The concurrent presence of an equilibrium between folded and unfolded species
142 of Yfh1 at low ionic strength was proven by the co-existence of minor extra peaks which
143 disappear as soon as physiologic concentrations of salt are added.²¹

144

145 **Identification of residues consistent with or outliers from the global behaviour**

146 We correlated each amide resonance to the corresponding value of RAD, the parameter
147 introduced in Puglisi et al.,¹³ to pinpoint residues close to the hydrophobic core (**Table 1**). Of
148 the 68 residues selected, 39 had RAD <0.5, 37 with RAD <0.4, 33 with RAD <0.3, 24 with
149 RAD <0.2 and 11 RAD < 0.1 (**Table 1**). The residues with RAD<0.1 (henceforth called
150 RAD_0.1) were used to calculate the average. Comparison of the stability curves of the non-
151 overlapping amide resonances with this average showed that several residues with quite
152 different RAD values yield stability curves drastically different from the average (**Figures 1a**).
153 We next tried to classify the individual stability curves into those that matched well the average
154 RAD_1 curve ('well-behaved') and those that did not ('ill-behaved'). The curves for residues
155 in the hydrophobic core were in good agreement with the average curve (**Figures 1b**).

156



157

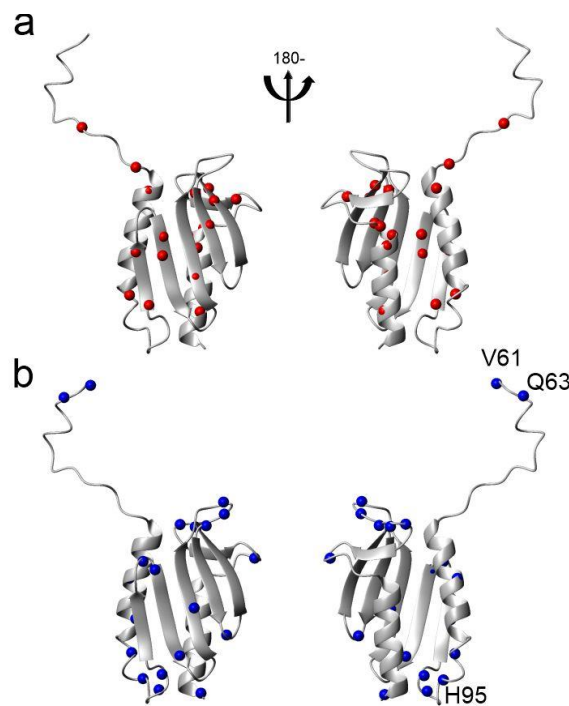
158 **Figure 1.** Comparison of single residue stability curves with the global RAD_0.1 best curve
 159 (dashed black). **a)** Stability curves of all observable isolated residues. **b)** Stability curves of
 160 residues with a RAD < 0.1. **c)** Stability curves of single residues for which the difference in the
 161 unfolding temperatures with respect to values of the reference curve (ΔT_m and ΔT_c) is on
 162 average below 1.5 °C **d)** Stability curves of single residues for which the difference in the
 163 unfolding temperatures with respect to values of the average curve (ΔT_m and ΔT_c) is on
 164 average above 3 K. For simplicity, colour coding is not the same in the different panels.

165

166 However, we could not find in general a clear-cut criterion to decide when the curves were not
 167 consistent with the average. We arbitrarily chose to set a cut-off at values of the unfolding
 168 temperatures (T_m and T_c) that differed, on average, less than 1.5 K from those corresponding
 169 to the average (RAD_0.1). These ΔT_m and ΔT_c differences are smaller than the variability that
 170 we had observed among different preparations and measurements of the same protein.^{2,4,7,8,13,22}

171 The residues selected according to this criterion are E71, E75, D78, L91, D101, L104, M109,
 172 T110, Y119, I130, L132, F142, D143, L152, L158, T159, D160 and K168 (**Figure 1c**). Most
 173 of the amide groups of the well-behaved residues are spread among well-structured secondary
 174 elements, but a few are in less ordered regions (**Figure 2a**). By the same token, we selected as
 175 ‘ill-behaved’ residues those whose T_m and T_c values differed from the average curve, on

176 average, more than 3 K with respect to the best curve RAD_0.1. Twenty-one residues (V61,
 177 Q63, H83, L88, S92, H95, C98, I99, G107, V108, I113, V120, N127, K128, Q129, L136,
 178 N146, G147, N154, K172, Q174) belong to this sub-set. Except for a few outliers, they are all
 179 in less structured regions (**Figure 2b**). Amongst these residues, V61, Q63, H95 which are
 180 positioned in flexible regions (either in the N-terminal tail or in a loop), are those with the
 181 largest shift of T_c . This behaviour is, however, not a general rule as some of the best-behaved
 182 residues reported in **Figure 1c** are not in regular secondary structure elements confirming the
 183 complexity of the system under study.



184
 185 **Figure 2.** Distribution of residues on the structure of Yfh1 (pdb id 2fql). a) Distribution of the
 186 nitrogen atoms of residues for which the difference in the unfolding temperatures with respect
 187 to values of the RAD_0.1 curve (ΔT_m and ΔT_c) is on average below 1.5 K. b) Distribution of
 188 the N atoms of residues for which the difference in the unfolding temperatures with respect
 189 to values of the average curve (ΔT_m and ΔT_c) is on average above 3 K. Indicated explicitly are
 190 the three residues whose stability curve is most shifted to lower temperatures with respect to
 191 the average RAD_0.1. The structure pairs are rotated by 180 degrees around the y axis.

192
 193 The stability curves of the residues that differ from the average (**Figure 1d**) have an
 194 important peculiarity: most stability curves show a moderate decrease of T_m ($\Delta T_m < 0$) and a
 195 large decrease of T_c ($\Delta T_c \ll 0$) from the average. This finding would imply that the
 196 corresponding transition temperatures for the heat and cold unfolding point to a decreased
 197 stability for heat denaturation but an increased stability for cold denaturation.

198
 199 **Evaluating the contribution of errors**

200 To make sure that the effect is beyond experimental errors, we reasoned that three phenomena
201 could potentially lead to erroneous populations, $f_F(T)$ and $f_U(T)$, and thus stability curves: 1)
202 the folding exchange dynamics leading to a time-dependent fluctuation of the ^1H chemical shift
203 and loss of intensity during the INEPTs of the ^{15}N -HSQC, 2) differential intrinsic relaxation
204 rates in the folded and unfolded states, and 3) exchange of the detected amide protons with the
205 bulk solvent. We thus performed simulations to evaluate how much these phenomena could
206 influence the resulting curves (for a more detailed discussion see **Suppl. Mat.**). We found that,
207 although the three contributions affect the derived populations, the stability curves that are
208 naïvely calculated from the intensities observed in the NMR spectra as $\widetilde{\Delta G}(T) =$
209 $-RT \ln((1 - I_f)/I_f)$, where I_f is the peak intensity of the folded species, recapitulate the
210 general features of the expected stability curve, $\Delta G(T)$. Of particular interest is that the
211 temperature of maximum stability T_S (so called because it corresponds to zero entropy of the
212 stability curve), is well reproduced despite the deviations observed for the other parameters
213 (**Figure S4 of Suppl. Mat.**).

214 Our observations are thus beyond experimental error and indicate that the mechanisms
215 of the two unfolding processes, at high and low temperatures, are intrinsically different in
216 agreement with Privalov's theory.¹

217

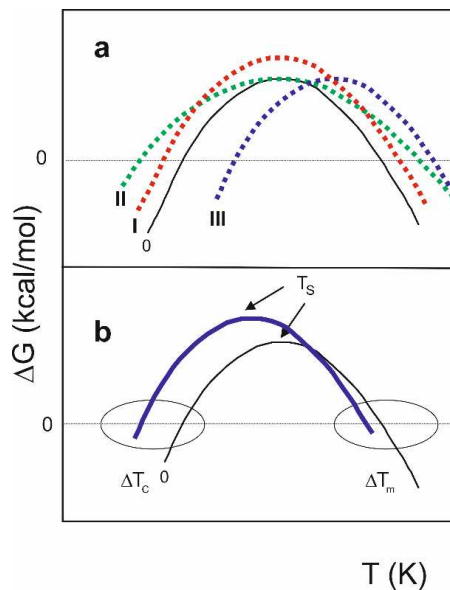
218 **A possible classification of the outliers**

219 The negative values of ΔT_m and ΔT_c observed for some residues (**Figure 1d**) imply that also
220 the temperature of maximum stability T_S for these residues is lower than that observed for the
221 best average RAD_0.1. A shift of T_S towards higher temperature values, when studying several
222 cases of thermophilic proteins, was attributed by Razvi & Scholtz²³ to a decrease in the entropy
223 difference in unfolding. Obviously, a *decrease* of T_m or T_c caused by shifting the T_s to lower
224 temperatures is connected to an increase in the entropy difference. This interpretation is based
225 on the classification by Nojima et al.²⁴ of the main mechanisms of changing the thermal
226 resistance, that is the resistance of heat to cross a material, of a protein. According to the rough
227 classification of Nojima et al.,²⁴ altered thermostability can be achieved thermodynamically in
228 three extreme cases (**Figure 3**). Real situations might of course contain mixtures of the three
229 possibilities.

230 According to mechanism I, when ΔH_S (the change in enthalpy measured at T_S) increases,
231 the stability curve retains the same shape, but with greater ΔG values at all temperatures. With
232 mechanism II, a decreased ΔC_p leads to a broadened stability curve retaining the same

233 maximum, because the curvature of the stability curve is given by $\frac{\partial^2 \Delta G}{\partial T^2} = -\frac{\Delta C_p}{T}$.¹⁸ According
 234 to mechanism III, the entire curve can shift towards higher or lower temperatures. It is possible
 235 to show¹ that:

$$236 \quad T_s = T_m \cdot \exp\left[-\frac{\Delta S_m}{\Delta C_p}\right] = T_m \cdot \exp\left[-\frac{\Delta H_m}{T_m \cdot \Delta C_p}\right]. \quad (1)$$



237
 238 **Figure 3.** Mechanisms that influence stability curves of a protein (adapted from Nojima
 239 et al, 1977). **a)** Dependence of the difference of free energy between unfolded and folded
 240 states (ΔG) of a hypothetical protein vs temperature (T) (curve 0). Mechanism I illustrates
 241 the effect of increasing ΔH_S (curve I). Mechanism II shows the effect of reducing ΔC_p
 242 (curve II). Mechanism III shows the shift of the whole stability curve towards higher
 243 temperatures caused by decreasing ΔS_m (curve III). **b)** A combination of the three
 244 mechanisms. The solid blue curve, with a prevalent low shift of T_s , corresponds
 245 qualitatively to the cases of Yfh1 reported in **Figure 1d**.

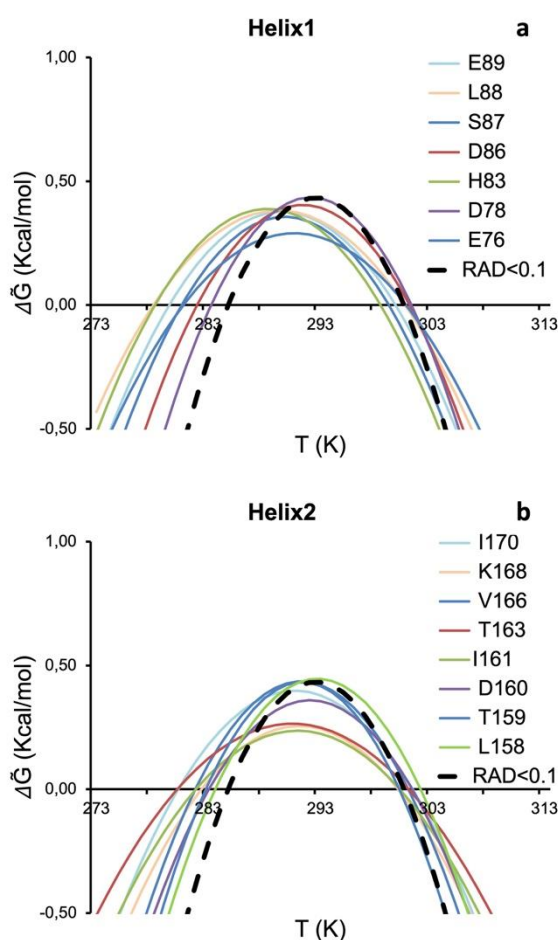
246
 247 Increasing the difference in entropy between the folded and unfolded states (ΔS_m) can shift
 248 values of T_s towards lower temperatures. Most of the curves in **Figure 1d** do not correspond
 249 to a single mechanism, but to a combination of them (**Figure 3b**). Nevertheless, all curves are
 250 shifted towards lower values of T_s and larger low-temperature differences correlate well with
 251 less ordered regions of the structure. It is thus not surprising to find this behaviour for residues
 252 at the N- and C-termini (Q63 and K172) or in connecting loops (G107, N127, N146 and N154)
 253 which are bound to be flexible.²⁵ More surprising is, however, to find amongst these residues
 254 also V120 which is right in the middle of the beta sheet. While we have not a definite

255 explanation for this observation at the moment, it could indicate a local frustration point in this
256 region.

257

258 Exploring the correlation between stability and secondary structure elements

259 We have previously shown that, in addition to the criteria of depth and exposition, an
260 alternative selection of residues over which average populations might be based on elements
261 of regular secondary structure.¹³ It is now possible to analyse the behaviour of each secondary
262 structure element. Of the 68 residues selected, 35 were in secondary structure elements (15 in
263 alpha helices, 20 in beta sheets). The largest number of residues of secondary structure traits
264 whose resonance is accessible belongs to the two helices (**Figure 4**).



265

266 **Figure 4.** Stability curves of residues belonging to secondary structure elements. **a)** Helix 1.
267 **b)** Helix 2. Residues are labelled with single letter code. The average stability curve is shown
268 as black dashed line.

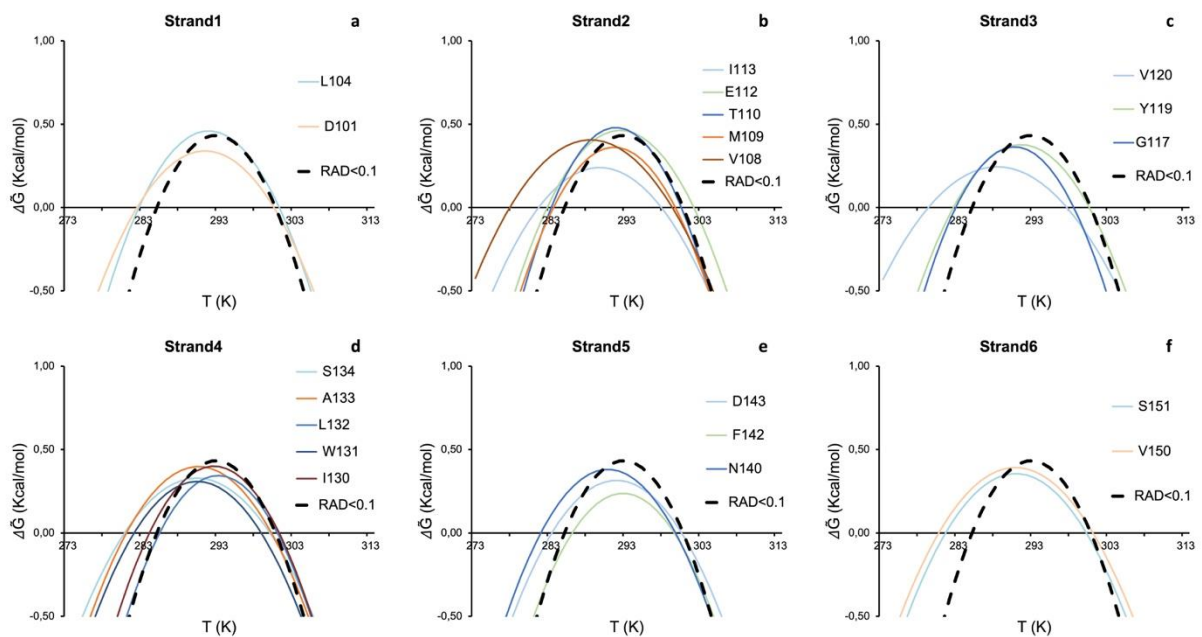
269

270 Several resonances have stability curves far from the reference one (dashed black curve of
271 RAD_0.1). These are those of His83 and Leu88 for helix 1 (**Figure 4a**). All the others are in
272 fair agreement with the average curve. The best-behaved residue (Asp78) is located at the end

273 of the helix with its amide groups in the buried side of the helix. For helix 2, the worst
 274 agreement is found for Thr163 and Ile170, whereas the best agreement is for Leu158, Thr159,
 275 Asp160 and Lys168 (**Figure 4b**). This implies that residues of helix 2 with a good agreement
 276 are distributed over the whole secondary structure element. Some residues of helix 2 have also
 277 lower stability curves which indicate a lower ΔH .

278 The number of residues belonging to beta strands for which it was possible to extract
 279 stability curves is more limited (**Figure 5**).

280



281

282 **Figure 5.** Stability curves of residues belonging to secondary structure elements. a) Strand 1.
 283 b) Strand 2. c) Strand 3. d) Strand 4. e) Strand 5. f) Strand 6. Residues are labelled with single
 284 letter code. The average stability curve is shown as black dashed line.

285

286 The best agreement was found for Leu104 of strand 1, Met109 and Thr110 of strand 2, Tyr119
 287 for strand 3, Ile130 and Leu132 of strand 4 and Phe142 and Asp143 of strand 5.

288

289 **The behaviour of tryptophan side chains**

290 We then looked into the possibility of following the process of unfolding and calculating
 291 thermodynamic parameters using the tryptophan side chains. This choice directly parallels
 292 studies based on following the process of unfolding by fluorescence using the intrinsic
 293 tryptophan fluorescence.²⁶ Yfh1 has two tryptophans: W131 is fully exposed to the solvent
 294 whereas W149 is buried. Both residues are fully conserved throughout the frataxin family and
 295 the two side chain resonances are clearly identifiable (**Figure S5a of Suppl. Mat.**). We
 296 calculated the thermodynamic parameters for the side chain indole groups of both residues by

297 the same procedure outlined for main chain NHs, generating first a stability curve. The
298 resonance of W149, which could potentially be more interesting, could not be used for
299 quantitative measurements because the temperature dependence of its volume yields a stability
300 curve very different from the others (**Figure S5b of Suppl. Mat.**) and leads to impossible
301 fitting parameters. This might be explained by the co-existence of folded and partially unfolded
302 species in equilibrium with each other in solution. As a consequence, the indole of W149
303 resonates both at 9.25 and 127.00 ppm (folded species) and at ca. 10.05 and 129.20 ppm (split
304 into three closely adjacent peaks, unfolding intermediates) (**Figure S5a of Suppl. Mat.**). As
305 previously proven experimentally, the resonances of the unfolding intermediates disappear
306 upon addition of salt (Figure 1, panel A and B in Vilanova et al.²¹ These resonances are also
307 at the same chemical shifts observed for the tryptophan indole groups at low and high
308 temperature where however the three signals collapse into one (**Figure S1 of Suppl. Mat.**).
309 The complex equilibrium between different species could thus explain the ill-behaviour of the
310 corresponding stability curve of this residue.

311 The behaviour of the resonance of the exposed W131 side chain is instead fully consistent with
312 that of RAD_0.1 and also with the original curve calculated from 1D NMR data² (**Table 1**).
313 On the whole, these results exemplify well the complexity of the selection choice of the
314 unfolding reporter and advocate in favour of a wholistic analysis of all the available data.

315

316 **Discussion**

317 The *de facto* demonstration that it is possible to reliably measure the thermodynamic
318 parameters of protein unfolding by 2D NMR spectroscopy¹³ has opened a new territory to study
319 protein unfolding at atomic resolution using site-specific information. Following protein
320 folding/unfolding looking at specific residues rather than obtaining an average overall picture
321 is not a novelty. Despite some intrinsic limitations, fluorescence has, for instance, been used
322 for decades to probe protein unfolding following the intrinsic tryptophan fluorescence.^{26,27}
323 Another elegant, although sadly still underexploited technique able to report local behaviour at
324 the level of specific residues is chemically induced dynamic nuclear polarization (CIDNP),
325 first introduced to the study of proteins by Robert Kaptein.²⁸ This technique allows the selective
326 observation of exposed tryptophans, histidines and tyrosines. In protein folding, it was, for
327 instance, used to characterize the unfolded states of lysozyme^{29,30} and the molten globule
328 folding intermediate of α -lactalbumin.^{31,32} Real-time CIDNP was also used to study the
329 refolding of ribonuclease A³³ and HPr.³⁴ The only drawback of this technique is that, as in
330 fluorescence, the information is limited to specific aromatic residues.

331 Another important technique that reports on protein unfolding at the single residue level
332 is stopped-flow methods coupled with NMR^{35,36} or mass spectrometry measurements³⁷ of
333 hydrogen exchange. In a classic paper,³⁸ Dobson and co-workers described, for instance, NMR
334 experiments based on competition between hydrogen exchange as observed in COSY spectra
335 and the refolding process. The authors concluded that the two structural domains of lysozyme
336 followed two distinct folding pathways, which significantly differed in the extent of
337 compactness in the early stages of folding. Similar and complementary conclusions could be
338 reached by integrating NMR with mass spectrometry.³⁷ While these studies retain their solid
339 importance, the possibility of following the resonance intensities also by HSQC spectra may
340 provide a more flexible tool to obtain detailed information on unfolding, as this technique
341 reports on the exchange regime but also, implicitly, on the chemical environment. The use of
342 2D HSQC had been discouraged by the non-linear relationship between peak intensity (or
343 volume) and populations with temperature as the consequence of relaxation, imperfect pulses,
344 and mismatch of the INEPT delay with specific J-couplings. We have previously suggested an
345 approach to compensate for these effects and demonstrated that the non-linearity does not affect
346 the spectra of Yfh1,¹³ even though these conclusions might be protein dependent.

347 Here, we used the approach developed in our previous work¹³ to analyse individual
348 stability curves for most of the residues of Yfh1. Our analysis is highly complementary to the
349 single residue information that may be obtained through HDX by NMR or mass
350 spectrometry.^{39,40} A clear advantage of the current approach is the availability of signals of
351 almost all residues and the relative simplicity of the analysis.

352 We noted that Yfh1 shows a multitude of events on top of the overall folding/unfolding.
353 We observed that the behaviour of the individual stability curves is not distributed uniformly
354 along the sequence. Residues can be clearly divided into two groups, i.e. those consistent with
355 the average behaviour of an all-or-none mechanism of unfolding and those differing, even
356 strongly, from the best average RAD_0.1. This finding alone proved that it is not possible to
357 measure stability using a single residue without a careful evaluation of the role of the specific
358 residue in the protein fold. This conclusion is partially mitigated by our results on the
359 parameters obtained for a tryptophan indole. However, in the whole, also for these side chains
360 it may be difficult, *a priori*, to infer which tryptophan is more reliable. We showed that, of the
361 two tryptophans present in Yfh1 only the fully exposed W131 is suitable for the analysis. Our
362 results thus demonstrate that unfolding studies based on fluorescent measurements using the
363 intrinsic fluorescence of tryptophan should always be taken with a pinch of salt: in many cases
364 no independent controls are feasible to evaluate the accuracy of the results. The possibility of

365 using 2D NMR and the introduction of the easily approachable RAD parameter may assist in
366 this choice in future studies.

367 Analysis of individual secondary structure elements, i.e. helices and strands, showed that
368 there is no clear hierarchy among them, and there is no indication that any of the elements
369 undergoes disruption before the others, either at high or low temperature. This implies that,
370 overall, the folding/unfolding of the core of Yfh1 can be described as a single, highly
371 cooperative event, but not all residues could be used for following the transition. It will be
372 interesting in the future to study lysozyme to have an example in which two subdomains unfold
373 independently.³⁸ In addition to information on regular secondary structure elements, our
374 analysis yielded also interesting information on less ordered traits. Intrinsically flexible
375 elements, i.e. regions characterized by multiple conformers, can be identified unequivocally by
376 their thermodynamic parameters, without recurring to interpretative mechanisms.

377 Another important point is that we observed a clear difference between parameters
378 corresponding to the cold and the heat denaturation processes: residues that are outliers from
379 the average stability curve tend to have a strong stabilization effect at low temperature and a
380 weaker destabilising effect at high temperature. This is a strong confirmation that the
381 mechanisms of the two transitions are intrinsically different according to the mechanism of
382 cold unfolding proposed by Privalov. In this model, cold denaturation is intimately linked to
383 the hydration of hydrophobic residues of the core¹ and with his suggestion that the disruption
384 of the hydrophobic core at low temperature would be caused by the hydration of hydrophobic
385 residue side chains of the core, whereas the high temperature transition is mainly linked to
386 entropic factors, consistent with the increase of thermal motions when temperature is increased.
387 This is what we observed in our NMR analysis of Yfh1 and is in line with our previous evidence
388 that showed that the unfolded species at low temperature has a volume higher than the folded
389 species and of the high temperature unfolded species⁸ and that cold denaturation is caused by
390 a hydration increase.³

391 We also observed, more surprising, that some residues not belonging to the hydrophobic
392 core have T_{cs} appreciably lower than the average. A possible explanation for this behaviour is
393 that, at the temperature of global unfolding, corresponding to that of the average RAD_0.1 of
394 the deeply buried protein core, residues outside the hydrophobic core and in regions classified
395 as flexible could be more resilient against unfolding. This would imply that, at low temperature,
396 opening of the hydrophobic core and its disruption could happen before the collapse of external
397 and more exposed elements: the core would unfold in lowering the temperature whereas outer
398 turns could be affected last.

399

400 **Conclusions**

401 In conclusion, we have provided here a nice example of a protein that only apparently follows
402 a simple two-state (folded/unfolded) statistical model and for which a global denaturation curve
403 simply hides a profound intrinsic heterogeneity. We described in detail how the unfolding of
404 Yfh1 is a much more complex process than a two-step global unfolding both at high and low
405 temperature. Our data clearly show how, as recently advocated by Grassein et al.,¹⁴ local
406 nativeness is probe dependent and, as such, needs to be studied at the individual residue level.
407 The possibility of studying the process relied in our case on the nearly unique properties of
408 Yfh1 but also, more in general, on the use of NMR which is probably the most suitable
409 technique to analyse the contributions to the (un)folding process in a residue-specific manner.
410 We can certainly state that monitoring protein unfolding by the stability curves of individual
411 residues, as allowed by 2D NMR spectroscopy, yielded a much more informative picture than
412 what may have been obtained by any other traditional method. Our work thus paves a new way
413 to the study of protein unfolding that will need to be explored in the future using a number of
414 completely different systems to reconstruct a more complete picture of the complexity of the
415 process.

416

417 **Experimental session**

418 *Sample preparation*

419 Yeast frataxin (Yfh1) was expressed in BL21(DE3) *E. coli* as previously described.² To obtain
420 uniformly ¹⁵N-enriched Yfh1, bacteria were grown in M9 using ¹⁵N-ammonium sulphate as the
421 only source of nitrogen until an OD of 0.6-0.8 was reached and induced for 4 hours at 310K
422 with IPTG. Purification required two precipitation steps with ammonium sulphate and dialysis
423 followed by anion exchange chromatography using a Q-sepharose column with a NaCl
424 gradient. After dialysis the protein was further purified by a chromatography using a Phenyl
425 Sepharose column with a decreasing gradient of ammonium sulphate.

426

427 *NMR measurements*

428 2D NMR ¹⁵N-HSQC experiments were run on a 700 MHz Bruker AVANCE spectrometer. ¹⁵N-
429 labelled Yfh1 was dissolved in 10 mM Hepes at pH 7.5 to reach 0.1 mM with 0.1 mM
430 selectively ¹⁵N-labelled tyrosine CyaY. Spectra were recorded in the range 278-313 K with
431 intervals of 2.5 K and using the Watergate water suppression sequence.⁴¹ For each increment 8
432 scans were accumulated, for a total of 240 increments (TD). Spectra were processed with

433 NMRPipe and analysed with CCPNMR software. Gaussian (LB -15 and GB 0.1) and cosine
434 window functions were applied for the direct and indirect dimension respectively. The data
435 were zero-filled twice in both dimensions. Spectral assignments of Yfh1 were taken from the
436 BMRB deposition entry 19991.

437

438 *Selection of the amides to be used in our analysis*

439 Yfh1 contains 114 backbone amide protons. The first 23 residues are intrinsically disordered⁴²
440 and are part of the signal peptide for mitochondrial import, leading to 91 resonances in the
441 globular domain. Sixty-eight residues have non-overlapping and isolated resonances that allow
442 easily detectable and reliable volume calculation. Most of the excluded overlapping resonances
443 corresponded to disordered regions or to partially unfolded conformations in equilibrium with
444 the folded one in a slow exchange regime at room temperature.⁷

445

446 *Calculations of the RAD parameters*

447 The RAD parameter of the backbone amide nitrogen atoms of Yfh1 was calculated on the
448 crystallographic coordinates of a Tyr73-to-Ala mutant solved at 3.0 Å resolution (2fql, Kalberg
449 et al., 2006). This choice was dictated by the better resolution of this structure as compared to
450 an alternative NMR structure (2ga5) or to homology models. The mutation, that is at the very
451 beginning of the globular region of the protein, does not affect the structure of the protein as
452 demonstrated by comparison with other orthologs but changes the self-assembly properties of
453 the protein.⁴³ No hydrogen atoms were added. RAD was obtained using the software Pops
454 (<https://github.com/mathbio-nimr-mrc-ac-uk/POPS>) and SADIC
455 (<http://www.sbl.unisi.it/prococoa/>). As previously described (Puglisi et al., 2020), the RAD
456 parameter was defined according to the equation

$$457 \quad \text{RAD} = (D \times \text{RA} \times 100) \quad (5)$$

458 where D was the distance of an atom from the protein surface as calculated by the
459 program SADIC.⁴⁴ RA was the relative accessibility at atomic level RA defined as the ratio
460 between the exposed surface of a nitrogen atom with respect to that of the whole residue and
461 calculated by the software POP.⁴⁵ Most of the exposed residues had RAD values for the amide
462 nitrogens considerably higher than 0.5 and were excluded from the analysis (**Table 1**). The
463 curves obtained for individual resonances using RAD values between 0.5 and 0.1 had a lower
464 relative spread and a much better agreement with the CD curve (**data not shown**). The stability
465 curve and the thermodynamics parameters calculated from averaging amide volumes from
466 residues with a RAD value below 0.1 (RAD_0.1) were fully consistent with those calculated

467 from CD spectroscopy, within experimental error.¹³ Residues involved in secondary structures
468 were evaluated according to the DSSP program (<https://swift.cmbi.umcn.nl/gv/dssp/>).⁴⁶

469

470 *Calculation of the stability curves*

471 Volumes were calculated by summation of the intensities in a set box using the CCPNMR
472 software (<https://www.ccpn.ac.uk/v2-software/software>). The volumes were normalized by
473 dividing the volume of each peak of Yfh1 at a given temperature by the volume of CyaY Tyr69
474 amide peak at the same temperature as previously described.¹³ This normalization is meant to
475 filter out the non-linearity of the relationship between peak intensity (or volume) and
476 populations due to instrumental effects. The corrected volumes were transformed into relative
477 populations of folded Yfh1.

478 At each temperature, the fraction of folded protein was estimated by the equation

$$479 \quad f_U = (V_{\text{exp}} - V_U) / (V_F - V_U) \quad (2)$$

480 where V_{exp} is the measured volume, V_U is the volume of the unfolded state (assumed at 313 K),
481 and V_F is the volume of the folded (maximum value) taking into account that, as previously
482 proven,² at room temperature the unfolded forms of Yfh1 are in equilibrium with the folded
483 population present on average at 70%.

484 The fraction of folded, $f_F(T)$, and unfolded, $f_U(T)$, forms are a function of the Gibbs free energy
485 of unfolding, $\Delta G^\circ(T)$. If the heat capacity difference between the folded and unfolded forms,
486 ΔC_p , is assumed independent of temperature, the free energy is given by the Gibbs-Helmholtz
487 equation.⁴ The thermodynamic parameters T_m , ΔH_m and ΔC_p were derived by nonlinear least-
488 squares fitting using the Levenberg-Marquardt algorithm from the following equation and
489 omitting the points at 313 K for which, by definition from our assumption, f_U is equal to 1.

$$490 \quad f_U(T) = \frac{e^{-\frac{\Delta G^\circ(T)}{RT}}}{1 + e^{-\frac{\Delta G^\circ(T)}{RT}}} \quad (3)$$

491

492 in which T_m , ΔH_m and ΔC_p can be obtained by fitting the modified Gibbs-Helmholtz equation

$$493 \quad \Delta G = \Delta H_m \left[1 - \frac{T}{T_m} \right] + \Delta C_p \left\{ (T - T_m) - T \ln \left[\frac{T}{T_m} \right] \right\} \quad (4)$$

494 The curve corresponding to this equation is known as the stability curve of the protein.¹⁸ Other
495 parameters for low temperature unfolding, e.g. the low temperature unfolding (T_c), were
496 obtained from the stability curve.

497 Errors on the stability curves were evaluated propagating the errors from the covariance matrix
498 of the fit. In the representative fits reported in **Suppl. Mat. (Figures S6-S8)**, errors were
499 represented as gray lines calculated by the covariance method (Press et al., 1988). They
500 represent how well the measured populations (and thus ΔG) vs. temperature agree with the
501 equation for the stability curve. We reported six representative curves from the subset used to
502 calculate RAD_0.1 (**Figure S6**), four curves from the subset of Figure 1c (**Figure S7**), and four
503 curves corresponding to the best-behaved residues of the beta sheet (**Figure S8**). The curves
504 do not fully represent ΔG because, despite we assumed the protein completely unfolded at
505 313K, fitting showed that not all the residues reached a plateau of unfolding at high
506 temperature. We thus indicated the curves as $\widetilde{\Delta G}(T)$ to underline the distinction.

507

508 **Acknowledgments**

509 This manuscript is meant in celebration of the 80th birthday of Prof. Robert Kaptein. We thank
510 Geoff Kelly and Tom Frenkiel of the MRC Biomedical NMR Centre for helpful discussions
511 and technical support, Neri Niccolai and Franca Fraternali for help with their software SADIC
512 and PopS respectively. We also thankfully acknowledge the use of the NMR spectrometers at
513 the Randall unit of King's College London and the Francis Crick Institute for access to the
514 MRC Biomedical NMR Centre. The Crick Institute receives its core funding from Cancer
515 Research UK (FC001029), the UK Medical Research Council (FC001029) and the Wellcome
516 Trust (FC001029). The research was supported by UK Dementia Research Institute (RE1 3556)
517 that is funded by the Medical Research Council, Alzheimer's Society and Alzheimer's
518 Research UK.

519

520 **Author contributions**

521 All of the authors contributed to the research design and data analyses. R.P. performed most
522 of the experiments described here and of the extraction of the thermodynamic data. G.K. and
523 D.F.H. performed the simulations to estimate the accuracy of the derived stability curves and
524 evaluated the combined effects of the exchange between folded and unfolded, the differential
525 relaxation, and the hydrogen exchange. A.P. supported the work financially, provided the
526 protein material, and helped writing the manuscript. P.A.T. coordinated the work and wrote
527 the manuscript.

528

529 **Competing interests:** The authors declare no competing interests.

530

531

532 **References**

533

534 1. Privalov P. L. Cold denaturation of proteins. *Crit. Rev. Biochem. Mol. Biol.* **25**, 281-305.
535 (1990).

536 2. Pastore A., Martin S. R., Politou A., Kondapalli K. C. Stemmler T. & Temussi P. A.:
537 Unbiased cold denaturation: low- and high-temperature unfolding of yeast frataxin under
538 physiological conditions. *J. Am. Chem. Soc.* **129**, 5374-5. (2007).

539 3. Adrover, M., Martorell, G., Martin, S. R., Urosev, D., Konarev, P. V., Svergun, D. I.,
540 Daura, X., Temussi, P. & Pastore, A. The role of hydration in protein stability:
541 comparison of the cold and heat unfolded states of Yfh1. *J. Mol. Biol.* **417**, 413-24.
542 (2012).

543 4. Martin, S. R., Esposito, V., De Los Rios, P., Pastore, A. & Temussi, P. A.: The effect of
544 low concentrations of alcohols on protein stability: a cold and heat denaturation study
545 of yeast frataxin, *J. Am. Chem. Soc.* **130**, 9963–9970. (2008).

546 5. Sanfelice D., Politou A., Martin S. R., De Los Rios P., Temussi P. A. & Pastore A. The
547 effect of crowding and confinement: A comparison of Yfh1 stability in different
548 environments. *Phys. Biol.* **10**, 045002. (2013).

549 6. Pastore, A. & Temussi, P. A. The Emperor's new clothes: Myths and truths of in-cell
550 NMR. *Arch. Biochem. Biophys.* **628**, 114-122. (2017).

551 7. Sanfelice D., Puglisi R., Martin S. R., Di Bari L., Pastore A. & Temussi P. A. Yeast
552 frataxin is stabilized by low salt concentrations: cold denaturation disentangles ionic
553 strength effects from specific interactions. *PLoS One.* **9**, e95801. (2014).

554 8. Alfano, C., Sanfelice, D., Martin, S. R., Pastore, A. & Temussi, P. A. An optimized
555 strategy to measure protein stability highlights differences between cold and hot unfolded
556 states. *Nat. Commun.*, **8**, 15428 (2017).

557 9. Aznauryan, M., Nettels, D., Holla, A., Hofmann, H. & Schuler, B. Single-molecule
558 spectroscopy of cold denaturation and the temperature-induced collapse of unfolded
559 proteins. *J. Am. Chem. Soc.* **135**, 14040-3. (2013).

560 10. Bonetti, D., Toto, A., Giri, R., Morrone, A., Sanfelice, D., Pastore, A., Temussi, P.,
561 Gianni, S. & Brunori, M. The kinetics of folding of frataxin. *Phys. Chem. Chem. Phys.*
562 **16**, 6391-7. (2014).

563 11. Chatterjee, P., Bagchi, S. & Sengupta, N. The non-uniform early structural response of
564 globular proteins to cold denaturing conditions: a case study with Yfh1. *J. Chem. Phys.*
565 **141**, 205103. (2014).

566 12. Espinosa, Y. R., Grigera, J. R. & Caffarena, E. R. Essential dynamics of the cold
567 denaturation: pressure and temperature effects in yeast frataxin. *Proteins* **85**, 125-136.
568 (2017).

569 13. Puglisi R., Brylski Alfano C., Martin S. R., Pastore A. & Temussi P. A.:
570 Thermodynamics of protein unfolding in complex environments: using 2D NMR to
571 measure protein stability curves. *Commun. Chem.* **3**, 100. (2020).

- 572 14. Grassein P., Delarue P., Nicolai A., Neiers F., Scheraga H. A., Maisuradze G, G. & Senet
573 P. Curvature and Torsion of Protein Main Chain as Local Order Parameters of Protein
574 Unfolding. *J. Phys. Chem. B.* **124**, 4391-4398. (2020).
- 575 15. Danielsson, J., Mu, X., Lang, L., Wang, H., Binolfi, A., Theillet, F. X., Bekei, B., Logan,
576 D. T., Selenko, P., Wennerström, H. & Oliveberg, M. Thermodynamics of protein
577 destabilization in live cells. *Proc. Natl. Acad. Sci. U. S. A.* **112**, 12402-7. (2015).
- 578 16. Smith A. E., Zhou L. Z., Gorenssek A. H., Senske M. & Pielak G. J. In-cell
579 thermodynamics and a new role for protein surfaces. *Proc. Natl. Acad. Sci. U S A.* **113**,
580 1725-30. (2016).
- 581 17. Guseman, A. J., Speer, S. L., Perez Goncalves, G. M. & Pielak, G. J.: Surface Charge
582 Modulates Protein-Protein Interactions in Physiologically Relevant Environments,
583 *Biochemistry* **57**, 1681-1684. (2018).
- 584 18. Becktel, W. J. & Schellman, J. A. Protein stability curves, *Biopolymers* **26**, 1859-77.
585 (1987).
- 586 19. Levenberg, K.. A Method for the Solution of Certain Non-Linear Problems in Least
587 Squares. *Quart. Appl. Math.* **2**, 164–168. (1944).
- 588 20. Marquardt D. An Algorithm for Least-Squares Estimation of Nonlinear Parameters.
589 *SIAM J. Appl. Math.* **1**, 431–441. (1963).
- 590 21. Vilanova B., Sanfelice D., Martorell G., Temussi P. A. & Pastore A. Trapping a salt-
591 dependent unfolding intermediate of the marginally stable protein Yfh1. *Front. Mol.*
592 *Biosci.* **1**, 13. (2014).
- 593 22. Sanfelice D., Morandi E., Pastore A., Niccolai N. & Temussi P. A. Cold Denaturation
594 Unveiled: Molecular Mechanism of the Asymmetric Unfolding of Yeast Frataxin,
595 *Chemphyschem.* **16**, 3599-602. (2015).
- 596 23. Razvi A. & Scholtz J. M. Lessons in stability from thermophilic proteins. *Protein Sci.*
597 **15**, 1569-78. (2006).
- 598 24. Nojima H., Ikai A., Oshima, T. & Noda, H.: Reversible thermal unfolding of
599 thermostable phosphoglycerate kinase. Thermostability associated with mean zero
600 enthalpy change. *J. Mol. Biol.* **116**, 429-42. (1977).
- 601 25. Halle, B. Flexibility and packing in proteins. *Proc. Natl. Acad. Sci. U. S. A.* **99**, 1274-9.
602 (2002).
- 603 26. Monsellier, E. & Bedouelle, H. Quantitative measurement of protein stability from
604 unfolding equilibria monitored with the fluorescence maximum wavelength. *Protein*
605 *Eng. Des. Sel.* **18**, 445-56. (2005).
- 606 27. Bolis, D., Politou, A. S., Kelly, G., Pastore, A. & Temussi, P. A. Protein stability in
607 nanocages: a novel approach for influencing protein stability by molecular confinement.
608 *J. Mol. Biol.* **336**, 203-12. (2004).
- 609 28. Kaptein, R., Dijkstra, K. & Nicolay, K. Laser photo-CIDNP as a surface probe for
610 proteins in solution. *Nature* **274**, 293-4. (1978).

611

- 612 29. Broadhurst, R. W., Dobson, C. M., Hore, P. J., Radford, S. E. & Rees, M. L. A
613 photochemically induced dynamic nuclear polarization study of denatured states of
614 lysozyme. *Biochemistry* **30**, 405-412. (1991).
- 615 30. Schlörb C., Mensch S., Richter C. & Schwalbe H. Photo-CIDNP reveals differences in
616 compaction of non-native states of lysozyme. *J. Am. Chem. Soc.* **128**, 1802-1803. (2006).
- 617 31. Improta, S., Molinari, H., Pastore, A., Consonni, R. and Zetta, L. Probing protein
618 structure by solvent perturbation of NMR spectra. Photochemically induced dynamic
619 nuclear polarization and paramagnetic perturbation techniques applied to the study of the
620 molten globule state of alpha-lactalbumin. *Eur. J. Biochem.* **227**, 87-96. (1995).
- 621 32. Lyon, C. E., Suh, E. S., Dobson, C. M. and Hore, P. J. Probing the exposure of tyrosine
622 and tryptophan residues in partially folded proteins and folding intermediates by
623 CIDNP pulse-labeling. *J. Am. Chem. Soc.* **124**, 13018-13024. (2002).
- 624 33. Day, I. J., Maeda, K., Paisley, H. J., Mok, K. H. & Hore, P. J. Refolding of ribonuclease
625 A monitored by real-time photo-CIDNP NMR spectroscopy. *J. Biomol. NMR.* **44**, 77-86.
626 (2009).
- 627 34. Canet, D., Lyon, C. E., Scheek, R. M., Robillard, G. T., Dobson, C. M, Hore, P. J. & van
628 Nuland, N. A. Rapid formation of non-native contacts during the folding of HPr revealed
629 by real-time photo-CIDNP NMR and stopped-flow fluorescence experiments. *J. Mol.*
630 *Biol.* **330**, 397-407. (2003).
- 631 35. Kim, P. S. & Baldwin, R. L. Intermediates in the folding reactions of small proteins,
632 *Annu. Rev. Biochem.* **59**, 631-60. (1990).
- 633 36. Roder H. & Wüthrich K. Protein folding kinetics by combined use of rapid mixing
634 techniques and NMR observation of individual amide protons. *Proteins* **1**, 34-42. (1986).
- 635 37. Miranker, A., Robinson, C. V., Radford, S. E., Aplin, R. T. & Dobson, C. M. Detection
636 of transient protein folding populations by mass spectrometry, *Science* **262**, 896-900.
637 (1993).
- 638 38. Miranker, A., Radford, S. E., Karplus, M. & Dobson, C. M. Demonstration by NMR of
639 folding domains in lysozyme, *Nature* **349**, 633-6. (1991).
- 640 39. Englander, S.W. & Mayne, L. Protein folding studied using hydrogen-exchange labeling
641 and two-dimensional NMR. *Annu. Rev. Biophys. Biomol. Struct.* **21**, 243-65. (1992).
- 642 40. Miranker, A., Robinson, C.V., Radford, S.E. & Dobson, C.M. Investigation of protein
643 folding by mass spectrometry. *FASEB J.* **10**, 93-101. (1996).
- 644 41. Piotto M., Saudek V. & Sklenár V.: Gradient-tailored excitation for single-quantum
645 NMR spectroscopy of aqueous solutions. *J. Biomol. NMR* **2**, 661-665. (1992).
- 646 42. Popovic M., Sanfelice, D., Pastore C., Prischi F., Temussi P. A. & Pastore A. Selective
647 observation of the disordered import signal of a globular protein by in-cell NMR: the
648 example of frataxins. *Protein Sci.* **24**, 996-1003. (2015).
- 649 43. Karlberg T., Schagerlöf U., Gakh O., Park S., Ryde U., Lindahl M., Leath K., Garman
650 E., Isaya G. & Al-Karadaghi S. The structures of frataxin oligomers reveal the
651 mechanism for the delivery and detoxification of iron. *Structure* **14**, 1535-46. (2006).

- 652 44. Varrazzo D., Bernini A., Spiga O., Ciutti A., Chiellini S., Venditti V., Bracci L. &
653 Niccolai N. Three-dimensional computation of atom depth in complex molecular
654 structures. *Bioinformatics* **21**, 2856-60. (2005).
- 655 45. Cavallo, L., Kleinjung, J. & Fraternali, F. POPS: A fast algorithm for solvent accessible
656 surface areas at atomic and residue level. *Nucleic Acids Res.* **31**, 3364-6. (2003).
- 657 46. Kabsch, W. & Sander, C. Dictionary of protein secondary structure: pattern recognition
658 of hydrogen-bonded and geometrical features. *Biopolymers* **22**, 2577-637. (1983).
- 659
- 660
- 661

662 **Table 1.** Thermodynamic parameters of the detectable residues. The average stability curve was obtained selecting
 663 the residues with RAD_0.1 indicated in the table in bold face (Puglisi et al., 2020).

	ΔH (Kcal/mol)	ΔS (Kcal/mol)	ΔC_p (Kcal/molK)	T_m (K)	T_c (K)	RAD
61 Val	19,9	0,067	1,58	298,4	273,9	48,20
63 Gln	21,1	0,072	2,24	294,0	275,6	3,64
64 Glu	27,7	0,093	3,30	298,0	281,5	2,52
65 Val	24,3	0,081	2,71	299,7	282,2	0,31
68 Leu	21,0	0,071	3,02	296,5	282,8	0,75
70 Leu	28,5	0,096	3,73	298,2	283,1	2,35
71 Glu	29,1	0,097	3,59	299,8	283,9	7,13
72 Lys	33,1	0,111	3,73	299,6	282,2	6,24
75 Glu	24,3	0,081	2,75	300,0	282,7	2,07
76 Glu	17,4	0,058	1,71	300,6	280,8	0,91
78 Asp	29,0	0,096	3,18	301,1	283,2	0,17
83 His	22,8	0,076	2,21	298,4	278,2	0,21
86 Asp	25,4	0,084	2,62	301,0	282,0	0,27
87 Ser	22,8	0,076	2,42	299,1	280,6	0,34
88 Leu	20,2	0,067	1,75	300,6	278,1	0,04
89 Glu	22,1	0,074	2,14	299,7	279,5	0,20
90 Glu	26,1	0,087	2,50	300,9	280,5	0,52
91 Leu	34,1	0,114	4,19	300,3	284,3	0,16
92 Ser	22,6	0,075	1,97	299,7	277,3	0,15
93 Glu	19,5	0,065	1,97	300,1	280,7	0,61
94 Ala	23,6	0,079	2,55	299,6	281,5	4,10
95 His	18,6	0,062	1,31	300,7	273,2	0,28
97 Asp	23,3	0,078	2,52	299,0	280,9	0,95
98 Cys	22,6	0,076	2,59	297,7	280,6	0,26
99 Ile	17,6	0,059	1,75	297,5	277,8	0,11
101 Asp	22,3	0,074	2,42	300,2	282,1	1,08
104 Leu	29,5	0,098	3,12	300,9	282,4	0,78
105 Ser	23,7	0,079	2,51	299,7	281,2	1,18
107 Gly	19,3	0,065	2,44	296,6	281,1	3,58
108 Val	22,3	0,075	2,03	299,0	277,5	0,50
109 Met	26,6	0,089	3,25	299,4	283,3	0,63
110 Thr	33,2	0,111	3,79	300,2	283,0	0,23
112 Glu	28,5	0,094	2,88	301,9	282,5	0,41
113 Ile	17,4	0,059	2,11	297,6	281,3	0,12
115 Ala	15,4	0,052	2,77	295,8	284,9	2,48
116 Phe	14,8	0,049	1,73	298,0	281,3	0,62
117 Gly	27,6	0,093	3,48	298,2	282,6	0,98
119 Tyr	24,9	0,083	2,72	300,3	282,3	0,22
120 Val	15,7	0,053	1,68	297,3	279,0	0,33
127 Asn	23,0	0,077	2,46	297,0	278,7	5,81
128 Lys	15,5	0,052	1,35	300,4	277,9	0,66
129 Gln	14,3	0,048	1,80	296,8	281,2	0,20
130 Ile	27,9	0,093	3,19	300,9	283,8	0,02
131 Trp	21,7	0,073	2,54	298,6	281,8	0,04
132 Leu	26,4	0,088	3,34	300,7	285,1	0,02
133 Ala	24,7	0,082	2,52	299,9	280,7	0,19
134 Ser	20,3	0,068	2,07	299,7	280,5	0,13
136 Leu	13,2	0,044	1,27	299,3	278,9	0,25
140 Asn	25,4	0,085	2,80	299,4	281,6	0,17
142 Phe	20,9	0,070	3,06	299,3	285,8	0,03
143 Asp	21,9	0,073	2,50	300,2	283,1	0,13
146 Asn	23,6	0,080	3,61	295,0	282,1	2,00
147 Gly	25,2	0,085	2,37	297,8	277,0	4,80
148 Glu	21,6	0,072	2,69	298,8	283,0	1,40
150 Val	22,9	0,076	2,20	300,7	280,4	0,03
151 Ser	22,7	0,076	2,39	299,9	281,3	0,05
152 Leu	32,2	0,107	3,87	300,0	283,7	0,16
154 Asn	21,9	0,074	2,40	295,1	277,2	1,14
158 Leu	29,1	0,096	3,11	301,9	283,6	0,03
159 Thr	29,8	0,099	3,38	300,0	282,8	0,09
160 Asp	23,6	0,078	2,55	301,2	283,1	0,28
161 Ile	15,4	0,051	1,66	300,1	281,9	0,09
163 Thr	15,2	0,051	1,44	300,9	280,2	0,15
166 Val	27,3	0,091	2,81	300,8	281,8	0,06
168 Lys	17,3	0,058	1,93	299,9	282,4	0,16
170 Ile	22,6	0,075	2,11	301,3	280,3	0,31
172 Lys	28,1	0,095	3,84	294,1	279,7	1,5
174 Gln	20,6	0,069	2,2	297,5	279,2	
131 Trp.sc	27,1	0,091	3,21	299,4	282,8	

Figures

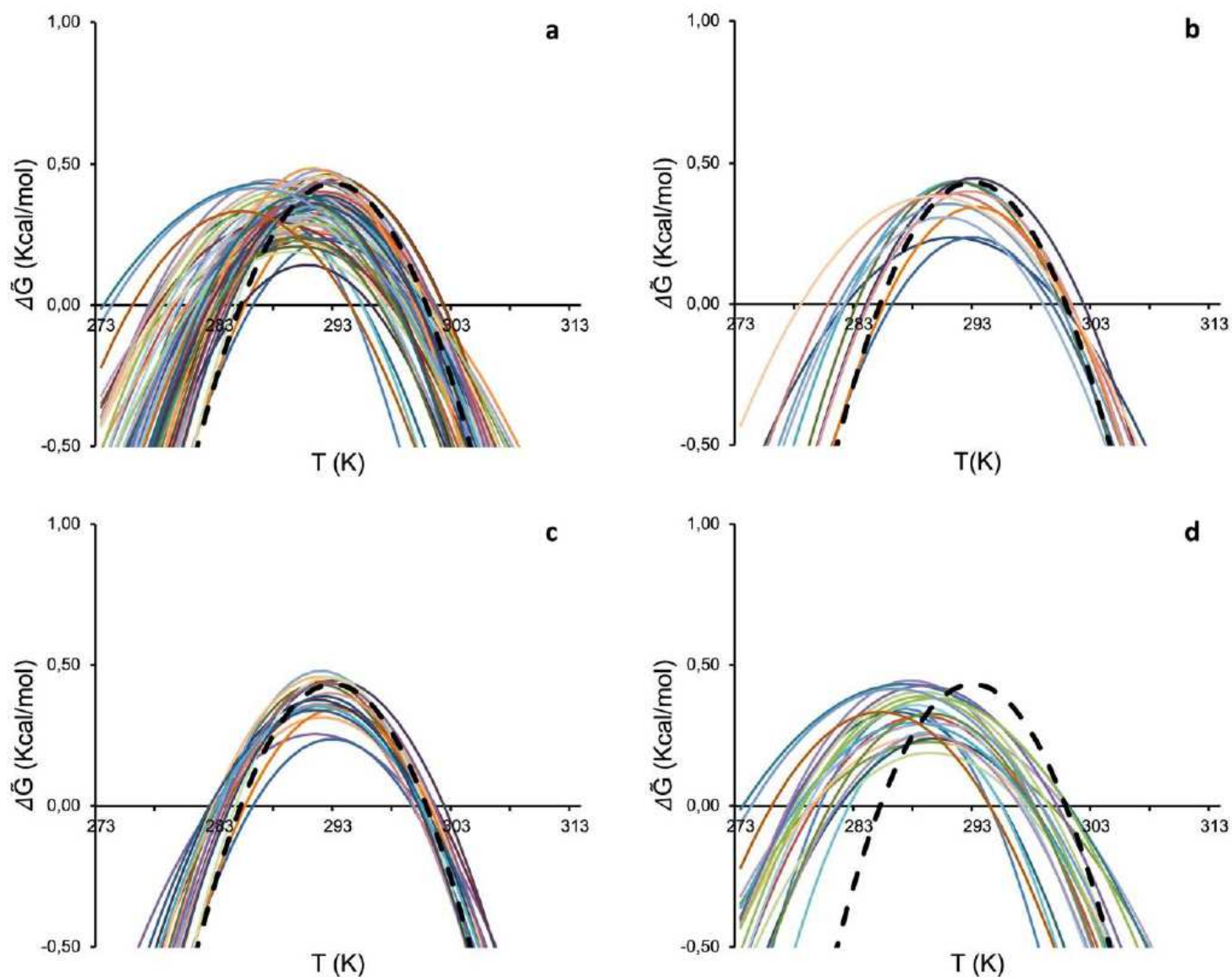


Figure 1

Comparison of single residue stability curves with the global RAD_{0.1} best curve (dashed black). a) Stability curves of all observable isolated residues. b) Stability curves of residues with a RAD < 0.1. c) Stability curves of single residues for which the difference in the unfolding temperatures with respect to values of the reference curve (ΔT_m and ΔT_c) is on average below 1.5 °C d) Stability curves of single residues for which the difference in the unfolding temperatures with respect to values of the average curve (ΔT_m and ΔT_c) is on average above 3 K. For simplicity, colour coding is not the same in the different panels.

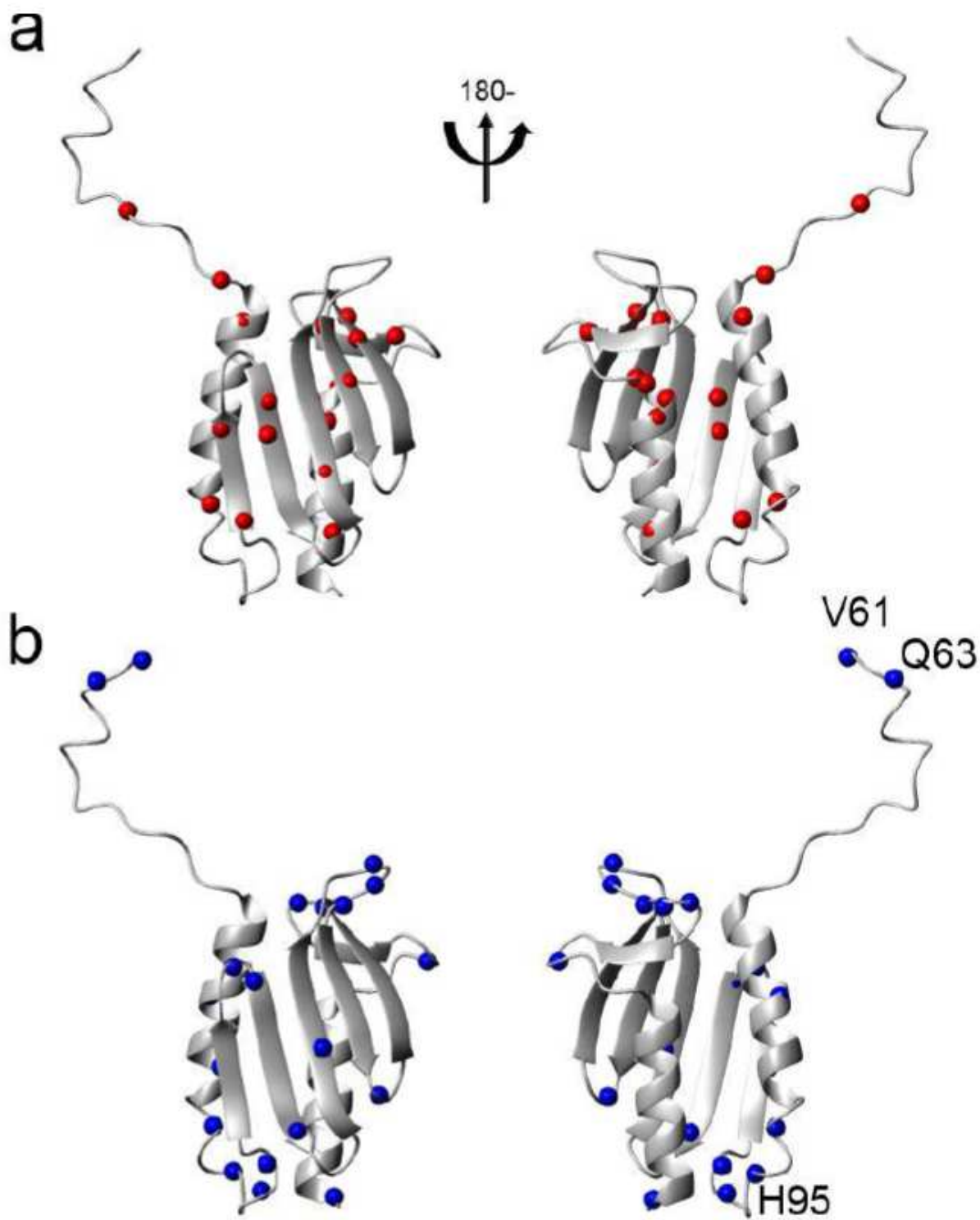


Figure 2

Distribution of residues on the structure of Yfh1 (pdb id 2fql). a) Distribution of the nitrogen atoms of residues for which the difference in the unfolding temperatures with respect to values of the RAD_0.1 curve (ΔT_m and ΔT_c) is on average below 1.5 K. b) Distribution of the N atoms of residues for which the difference in the unfolding temperatures with respect to values of the average curve (ΔT_m and ΔT_c) is on average above 3 K. Indicated explicitly are the three residues whose stability curve is most shifted to

lower temperatures with respect to the average RAD_0.1. The structure pairs are rotated by 180 degrees around the y axis.

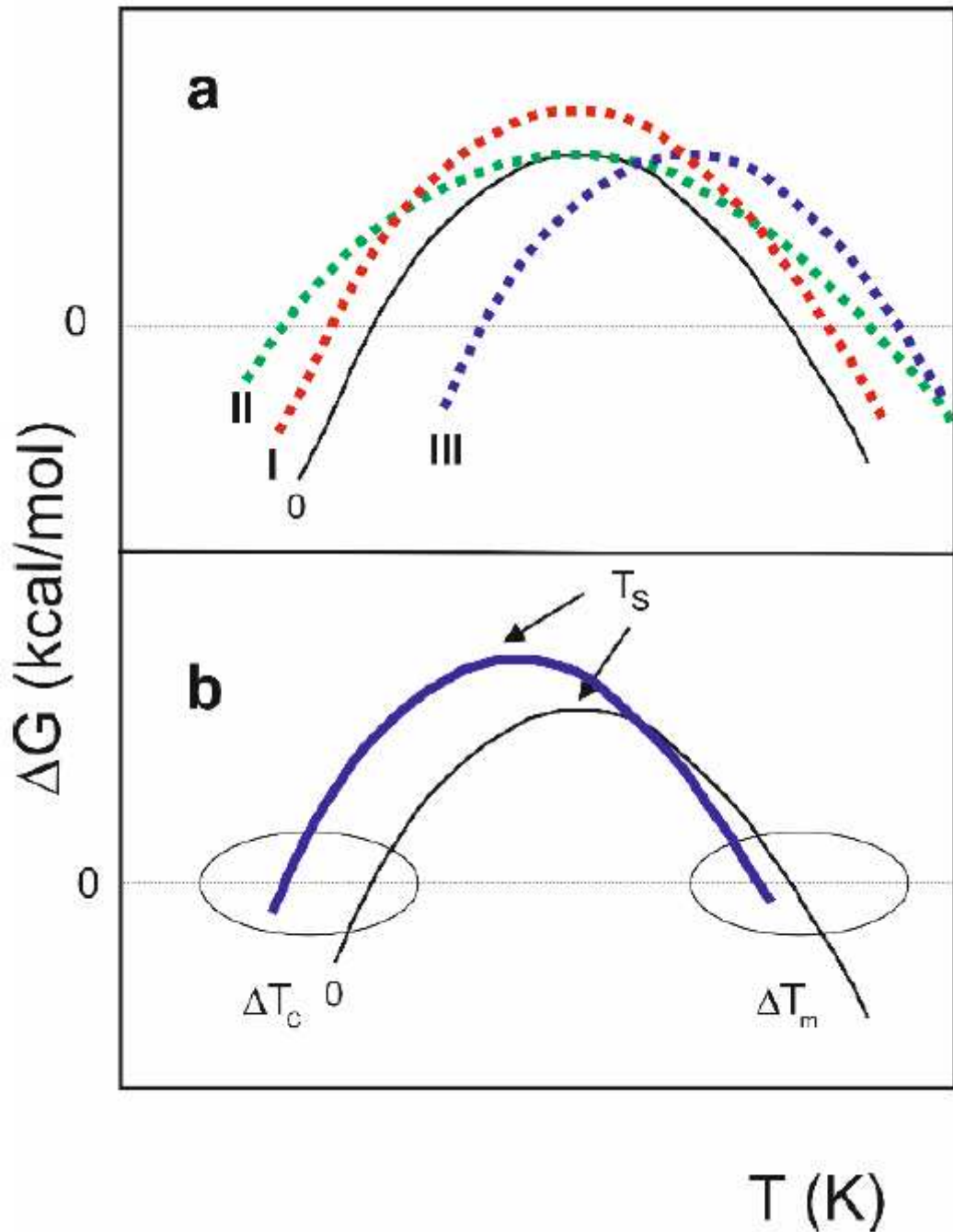


Figure 3

Mechanisms that influence stability curves of a protein (adapted from Nojima et al, 1977). a) Dependence of the difference of free energy between unfolded and folded states (ΔG) of a hypothetical protein vs temperature (T) (curve 0). Mechanism I illustrates the effect of increasing ΔH_S (curve I). Mechanism II shows the effect of reducing ΔC_p (curve II). Mechanism III shows the shift of the whole stability curve towards higher temperatures caused by decreasing ΔS_m (curve III). b) A combination of

the three mechanisms. The solid blue curve, with a prevalent low shift of TS, corresponds qualitatively to the cases of Yfh1 reported in Figure 1d.

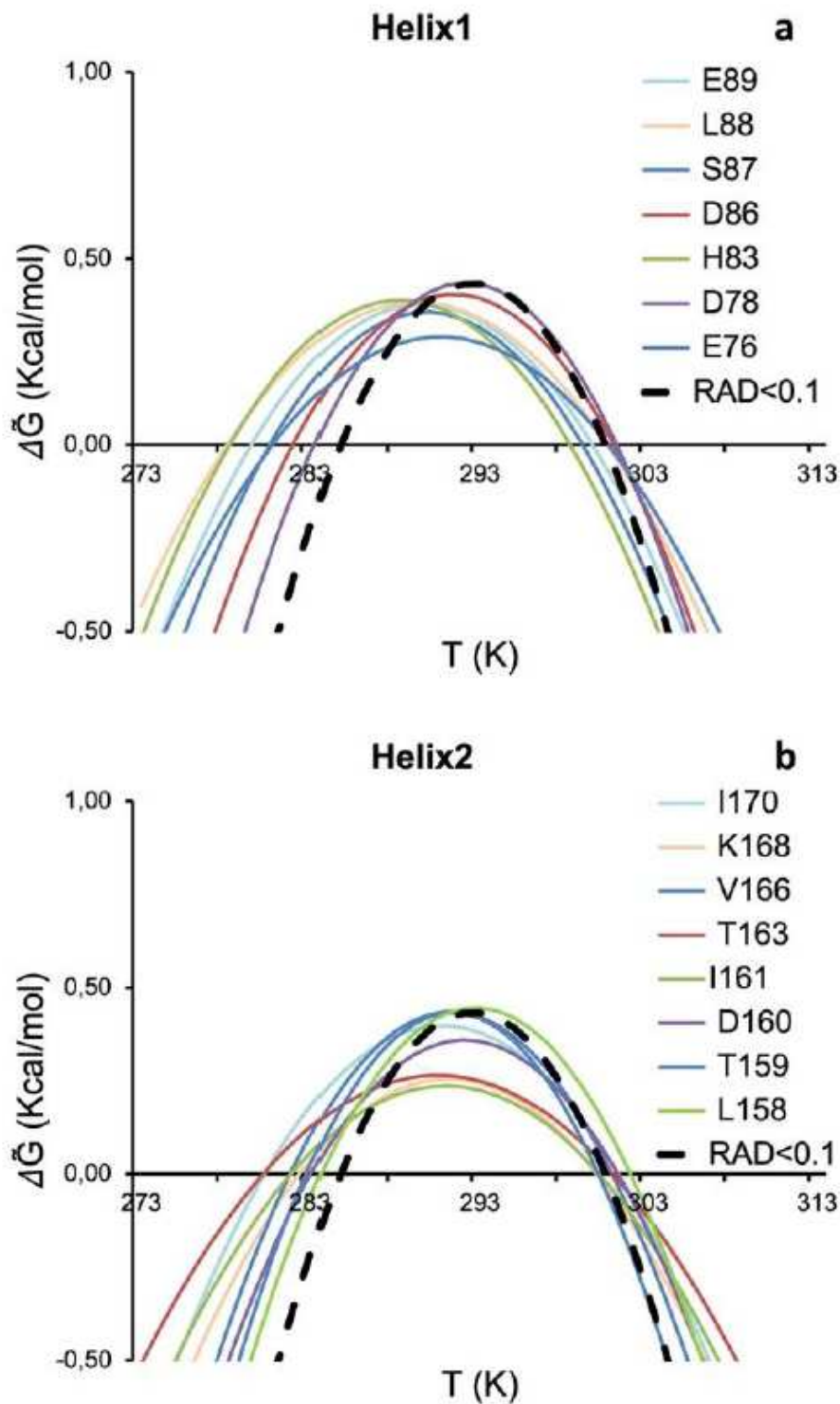


Figure 4

Stability curves of residues belonging to secondary structure elements. a) Helix 1. b) Helix 2. Residues are labelled with single letter code. The average stability curve is shown as black dashed line.

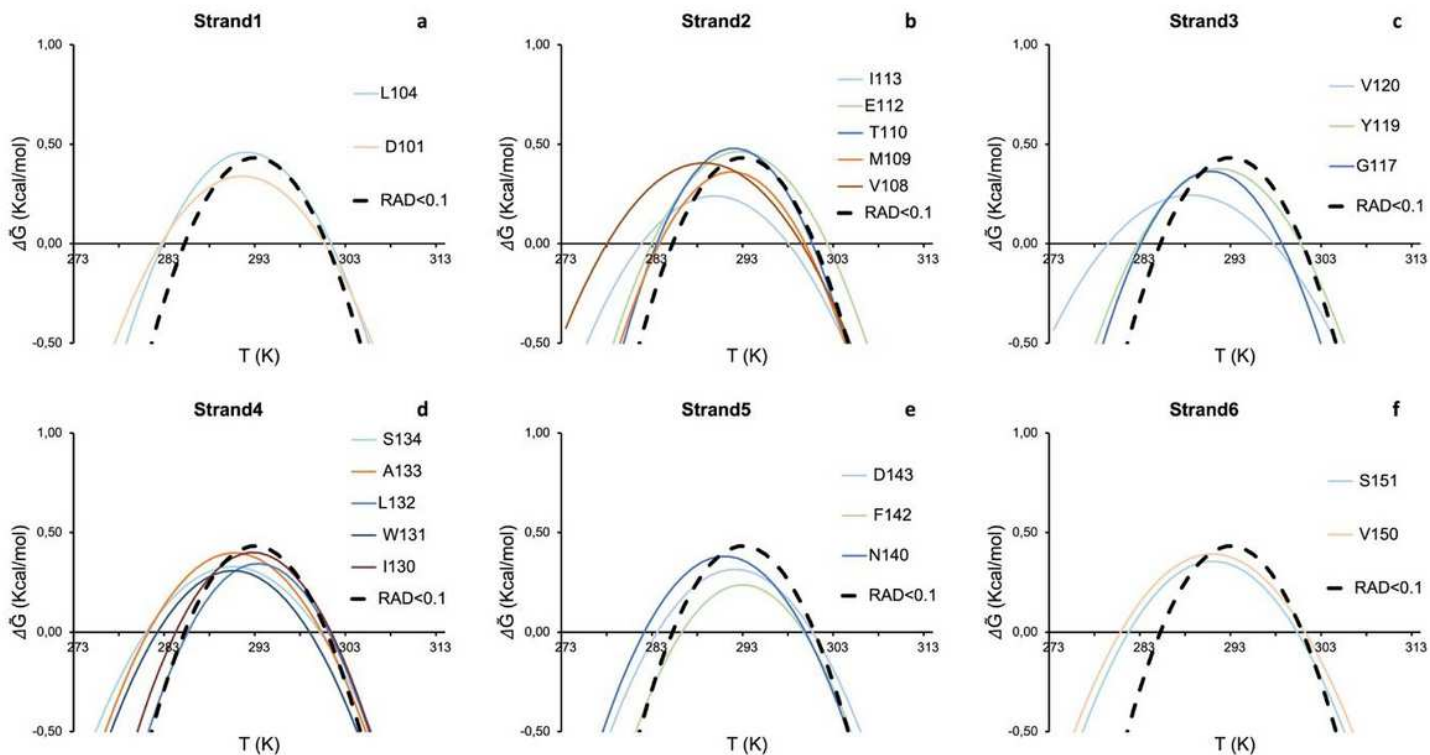


Figure 5

Stability curves of residues belonging to secondary structure elements. a) Strand 1. b) Strand 2. c) Strand 3. d) Strand 4. e) Strand 5. f) Strand 6. Residues are labelled with single letter code. The average stability curve is shown as black dashed line.

Supplementary Files

This is a list of supplementary files associated with this preprint. Click to download.

- [SupportingInformation.pdf](#)